Exploring the spin states of ^{90}Zr populated by (*p,p'*), (*p,d*), and (*p,t*) reactions

S. Ota[1a], J.T. Burke[1], R.J. Casperson[1], J.E. Escher[1], R.O. Hughes[1], J.J. Ressler[1], N.D. Scielzo[1], I.J. Thompson[1], R.A.E. Austin[2], B. Abromeit[3], N.J. Foley[3], E. McCleskey[3], M. McCleskey[3], H. I. Park[3], A. Saastamoinen[3], and T. J. Ross[4]

[1]*Lawrence Livermore National Laboratory, Physics and Life Science Directorate, Livermore, CA 94551, USA*
[2]*St. Mary's College, Halifax, Nova Scotia, Canada*
[3]*Texas A&M University, Cyclotron Institute, College Station, TX 77840, USA*
[4]*University of Kentucky, Department of Chemistry, Lexington, KY 40506, USA*

Abstract. The ^{90}Zr nucleus was produced by three different reactions: ^{90}Zr(*p,p'*), ^{91}Zr(*p,d*), and ^{92}Zr(*p,t*), and the spin-parity (J^π) population of the ^{90}Zr states produced by these reactions was studied to investigate the surrogate reaction approach, which aims at indirectly determining cross sections for compound-nuclear reactions involving unstable targets such as ^{89}Zr(*n,γ*). Discrete γ-rays, associated with the de-excitation of ^{90}Zr and ^{89}Zr, were measured in coincidence with light ions at ^{90}Zr excitation energies extending above the neutron separation energy. Low-lying states populated by (*p,d*) and (*p,t*) reactions agreed well with the previous measurements. The measured γ transition systematics were used to gain insights into the J^π distribution of ^{90}Zr around the neutron separation energy and it was found that the (*p,p'*) reaction preferentially produces lower J states than (*p,d*) and (*p,t*) reactions in the studied energy region.

1 Introduction

Radiative neutron-capture (*n,γ*) cross sections at neutron energies of a few tens of keV to a few MeV are crucial inputs for nuclear-energy applications, astrophysical studies, and radiochemical applications. However, the cross sections for most short-lived isotopes remain poorly known due to their inaccessibility as target materials. To address this problem, various types of indirect methods to infer the (*n,γ*) cross sections have been investigated, such as the surrogate reaction method [1-4]. Also, approaches to obtain the γ-ray strength function to constrain the (*n,γ*) cross sections are being developed by taking advantage of mono-energetic γ-rays obtained from laser Compton back-scattering method [5], the Oslo method [6], and other techniques [7, 8].

The surrogate reaction method aims at determining neutron-induced reaction cross sections by accessing the compound nuclei of interest via an alternative reaction such as a transfer reaction or inelastic scattering involving stable beams and stable (or long-lived) targets. In a surrogate experiment, a nucleus produced via a direct reaction is assumed to subsequently equilibrate to form

---

[a] Corresponding author: ota2@llnl.gov

the same compound nucleus that is formed in the desired neutron-induced reaction. The outgoing particle from the surrogate reaction is detected in coincidence with an observable (e.g., a specific γ-ray transition) that is characteristic of the decay channel of interest and the measured coincidence probability is used to constrain the reaction cross section.

A primary difficulty in determining $(n,γ)$ cross sections is the difference in the spin-parity $(J^π)$ distributions of the compound nucleus created by the $(n,γ)$ and the surrogate reactions. The γ-ray emission of the compound nucleus can be quite sensitive to the initial $J^π$ distribution [9]. Therefore, in order to extract $(n,γ)$ cross sections from surrogate data, it becomes necessary to take into account the $J^π$ distribution of the decaying compound nucleus. When this distribution is known, the decay of the nucleus can be modelled and constraints on the desired $(n,γ)$ cross sections are obtained by fitting the decay model to observables from the surrogate experiment. Details about the modelling based on the γ-ray decay probabilities can be found in [10].

With this background, we studied spin states in the nucleus ^{90}Zr populated by ^{90}Zr$(p,p')^{90}$Zr, ^{91}Zr$(p,d)^{90}$Zr, ^{92}Zr$(p,t)^{90}$Zr reactions. The ^{90}Zr nucleus is well suited for benchmarking the surrogate approach. The low level densities in the Zr mass region due to the presence of closed proton and neutron shells, leads to a competition between γ decay and neutron emission that is sensitive to the $J^π$ distributions of the decaying compound nuclei and can be expected to be visible in the measured discrete γ-ray emission probabilities.
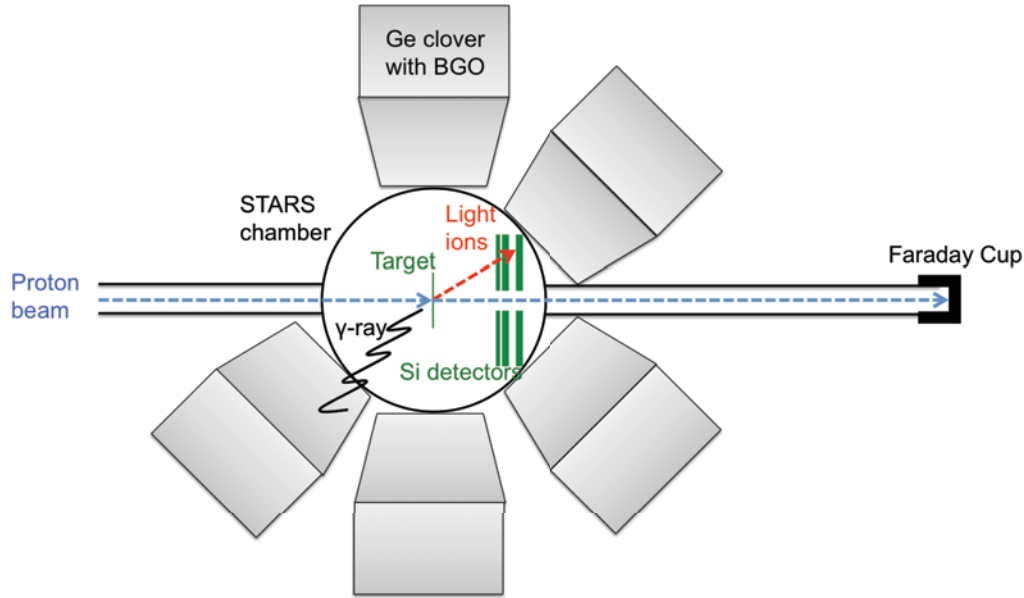
2 Experiment

The experiments were performed at the K150 Cyclotron facility at Texas A&M University. Enriched ^{90,91,92}Zr targets with thicknesses of 1.02, 1.01, and 0.960 mg/cm^2, respectively, were bombarded with a 28.56-MeV proton beam with an intensity of about 1.5 nA. Outgoing protons (for (p,p') reactions), deuterons (for (p,d)), and tritons (for (p,t)) were detected at forward angles. Measurements were run for 12, 36, and 84 hours for the experiments using the ^{90,91,92}Zr targets, respectively.

A schematic view of the experimental set up is shown in Fig. 1. The energy spectra and angular distribution of the light ions and prompt γ-rays were measured with the STARLiTeR detector system [11]. The STARLiTeR consists of three double-sided Micron S2 silicon detectors (referred to as *ΔE*, *E1*, and *E2* hereafter) which are each segmented into 24 rings (one side) and 8 wedges (the other side), allowing the measurement of charged-particle scattering angles. The thickness of the *ΔE*, *E1*, and *E2* detectors are 143 μm, 1000 μm, and 994 μm, respectively. The *ΔE*, *E1*, and *E2* detectors were located at 19.2 mm, 23.4 mm, and 33.8 mm from the target and were used to identify charged-particles from (p,p'), (p,d), and (p,t) reactions covering angles between 25-58°.

For γ-ray detection, five Bismuth Germanate Oxide (BGO) Compton-suppressed High Purity Germanium (HPGe) clover detectors surrounded the silicon chamber. The energy resolution and the total absolute photopeak efficiency were measured using calibrated γ-ray sources placed at the target position before and after the experiments. The typical energy resolution was 2 keV for energies below 500 keV increasing to 5 keV at 3 MeV. The efficiency of the array was 3.8% at 150 keV, 1.5% at 500 keV, and 0.5% at 2 MeV after addback was applied. The γ-ray energies were measured up to about 5 MeV.

Coincident particle-γ events were identified based on the time difference between particle and prompt γ-ray signals. Further details on the detector arrays, data-taking system, and data analysis can be found in [4] and references therein.

Figure 1. Schematic view of the experimental set up.

## 3 Spin population in low-lying states

3.1 Particle singles spectra

After particle identification using a conventional ΔE-range plot (see [3]), the detected particle energy was corrected for the recoil energy of the target nuclei and energy losses in the targets and dead layers of the Si detectors to obtain the total kinematic energy (E). The excitation energies (E_x) in ^{90}Zr can be determined from

$$E_x = E_b - E + Q, \tag{1}$$

where E_b, the beam energy, is 28.56 MeV, and Q-values for (p,p'), (p,d), and (p,t) reactions are 0, -4.969, and -7.346 MeV, respectively.

Fig. 2 shows the observed E distribution for ^{90}Zr(p,p'), ^{91}Zr(p,d), ^{92}Zr(p,t) reactions after correcting for backgrounds from Zr, C, and O contaminants. The full-width at half maximum (FWHM) for the ^{91}Zr(p,d) ground-state peak measured by the $\Delta E + E1 + E2$ detectors was about 300 keV. Similarly, the FWHM for the ^{92}Zr(p,t) ground-state peak measured by the $\Delta E + E1$ detectors was about 200 keV. This peak was observed at $E = 23.6$ MeV and 21.2 MeV for the ^{91}Zr(p,d) and ^{92}Zr(p,t) reactions, respectively, which agree well with the calculated values from Eq. (1).

In the ^{90}Zr(p,p') reaction, events with $E > 21.5$ MeV ($E_x < 7$ MeV) were mostly missed because these particles punch through the $E2$ detector. On the low-energy side, the events with $E < 7.5$ MeV ($E_x > 21.0$ MeV) were mostly cut off because these are stopped in the ΔE detector. Therefore, the energy range utilized in the ^{90}Zr(p,p') reactions is $E_x = 7.0$-21.0 MeV, which spans a 14-MeV energy region around the neutron separation energy of ^{90}Zr ($S_n = 11.97$ MeV). Similarly, the energy ranges utilized in ^{91}Zr(p,d) and ^{92}Zr(p,t) reactions are $E_x = 0$-15 MeV and $E_x = 0$-11 MeV, respectively. These are wide enough to study excitations around S_n although the energy region above S_n is missed in the ^{92}Zr(p,t) reactions.
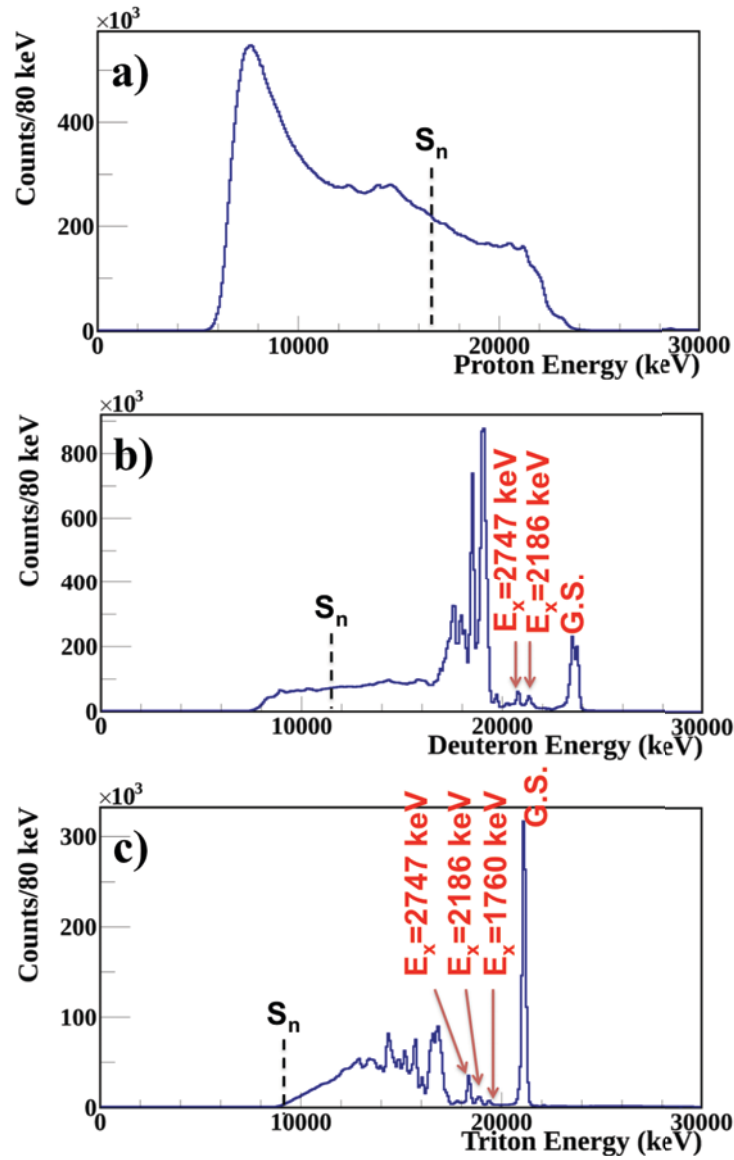
Figure 2. Particle singles spectra from a) ^{90}Zr(p,p ')^{90}Zr, b) ^{91}Zr(p,d)^{90}Zr, c) ^{92}Zr(p,t)^{90}Zr reactions.

From Fig. 2 b) and c), we can see different ways of populating low-lying levels at E_x < 3 MeV in ^{91}Zr(p,d), and ^{92}Zr(p,t) reactions. The first excited state (E_x = 1760 keV (0$^+$)) is not observed in ^{91}Zr(p, d), but is observed in ^{92}Zr(p,t). This supports the result by [9] in which the spectroscopic factor of this state was estimated to be < 0.001 and therefore the cross section for the state should be extremely small in the ^{91}Zr(p,d) reaction. The second excited state (E_x = 2.186 MeV (2$^+$)) is clearly seen in both reactions. The third excited state (E_x = 2.319 MeV (5$^-$)) is not seen in the (p,d) data, which agrees with the measured spectrum in [12]. However, as discussed later, it was found that this state was just not well separated from the E_x = 2.186 MeV state in the (p,t) data. The mixed peaks of the fourth and the fifth excited states (E_x = 2.739 (4$^-$) and 2.747 MeV (3$^-$), respectively) are also observed in both

reactions.

Several large peaks are observed around E_x = 4.0-6.5 MeV in Fig. 1 b) and at E_x = 4-8 MeV in Fig. 1 c). Although the limited energy resolution of the Si detectors do not allow for unambiguous structure information on these peaks, the particle-γ coincidence technique reveals the individual levels contributing to these peaks as described in following sections.

3.2 Particle-γ coincidence for (*p,d*) reaction

The particle-γ coincidence technique is of great help to identify the levels from which γ-rays are emitted with higher precision than is possible with the charged-particle measurements alone. Furthermore, since the γ-ray energies can be determined to ~ 1 keV, it is possible to assign these γ-rays to specific known levels at medium level density regions. A sophisticated ^{90}Zr(*n,n'*) experiment performed in the 2000's [13] reported more than 50 new levels and 170 γ-ray transitions below E_x = 5.8 MeV and greatly improved the information available on the excited states of ^{90}Zr. Here, the particle-γ coincidence technique was applied to study the peaks in Fig. 2 using the latest nuclear level information.

Fig. 3 a) shows the energy spectrum for deuterons in coincidence with γ-ray transitions from levels at E_x < 5.8 MeV in ^{90}Zr. As energies of the levels (E_i) which emit these γ transitions (*i*) are known from the literatures, the deuteron spectrum was created from these coincidence deuterons around the levels (typically collected from E_i ± 240 keV) taking into account the γ-ray branching ratios and detection efficiency. For instance, the γ-rays with the energies of 1656 and 3842 keV are emitted from the level of E_x =3842 keV (2$^+$) with the branching ratio of 0.145 and 0.855, respectively [13]. Then the deuterons in coincidence with the 1656 keV γ-ray are collected around E_x =3842 keV (E = 19.75 ± 0.24 MeV) correcting for the branching ratio (0.145) and the γ-ray detection efficiency. Similarly the deuterons in coincidence with 3842 keV γ-ray are collected at the same energy region and corrected for the branching ratio (0.855) and the efficiency. The sum of both events were considered to be the total deuteron singles count from E_x =3842 keV state (E = 19.75 MeV). The same procedure was performed for all the γ-ray transitions reported in [13].

To compare with the actual deuteron singles spectrum, the reconstructed deuteron spectrum was assumed to be Gaussian shape with the energy resolution (FWMH) of 200 keV as shown in Fig. 3 b). The low-lying excited state peaks such as E_x = 2186, 2747, 3308, and 3842 keV are well reproduced in both energy and intensity. The large peak at E_x = 4.5 MeV is well reproduced as well. It is remarkable agreement considering no angular correlation is taken into account in the reconstructed spectrum. The two large peaks at E_x = 5.5 MeV and E_x = 5.0 MeV are also well reproduced in energy, but intensities are both much reduced. These discrepancies in intensity come most likely from lack of data about discrete levels for excitation energies above 5 MeV. In fact, the reported number of levels above 5 MeV is only 32, which is clearly fewer than theoretically expected number of levels at this energy region.

Nevertheless, contributions to the two peaks at E_x = 5.5 MeV and 5.0 MeV are still explainable to some extent from the present data. Thus we can discuss some strongly populated levels for E_x = 4.0 - 5.8 MeV as follows. It turns out that the peak at E =19.0 MeV is comprised of E_x =4.541 (6$^+$, 26%), 4.454 (5$^+$,24%), 4.331 (3$^+$, 17%), 4.814 and 4.818 (3, and 3,4$^+$,11% for two), and 4.640 MeV (7,8, 10%) levels (percentage denotes contributions to the peak). Likewise, it was found that the peak at E = 18.5 MeV consists of E_x =5.060 (7$^+$, 56%), 4.992 (2 , 22%), 5.107 MeV (3,4$^+$, 15%) levels. It turns out that the peak at E =18.0 MeV dominantly consists of only 5.426 MeV (3) level although there remain uncertainties in the rest of the contributions as discussed above.
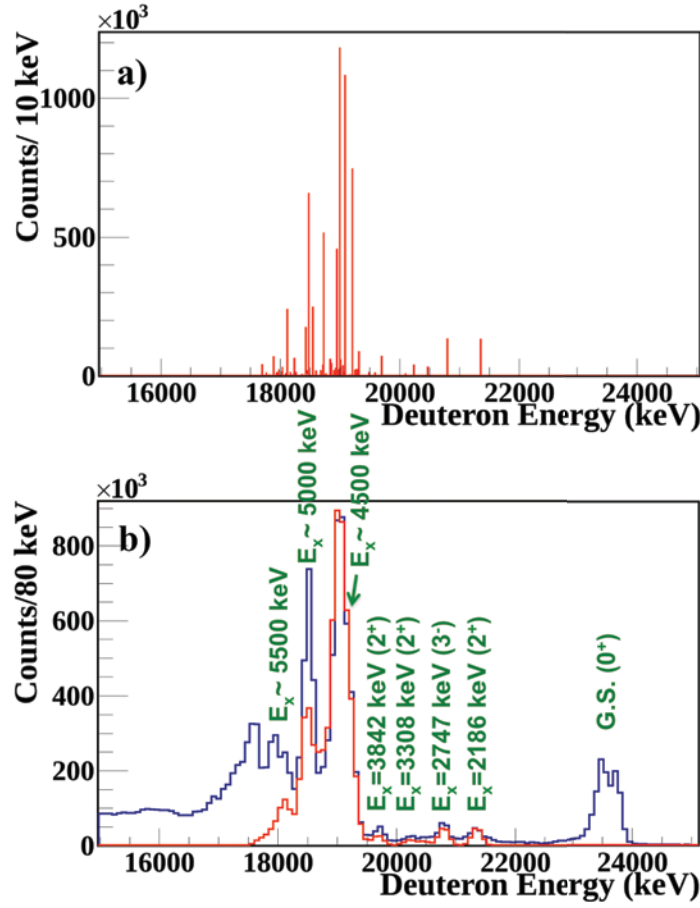
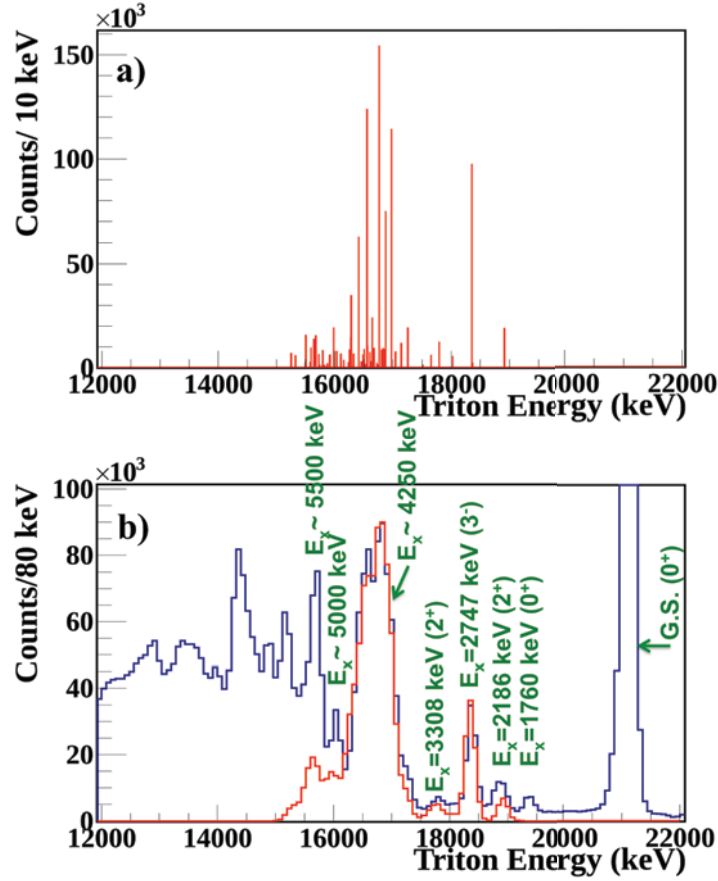**Figure 3.** a) Estimated contributions from individual states to the ^{91}Zr(p,d) spectrum (see text for details). b) Simulated deuteron singles spectrum from the estimation (red) and actual deuteron singles spectrum (blue).

Ball and Fulmer [12] measured a deuteron spectrum from ^{91}Zr(p,d) reactions between the ground state and E_x = 6.5 MeV in ^{90}Zr at 30° with a 31 MeV proton beam. They used a magnetic spectrograph with a typical energy resolution of 18 keV. However, the possible ambiguities in energy calibration (on order of 10 keV) was pointed out in [13] and this made it difficult for them to compare the levels found through (n,n') reactions with the levels reported by [12]. In the present work, the level energies were identified with 3-5 times better energy resolution than in the previous ^{91}Zr(p,d) measurement [12], it helps identify the states observed by [13]. The intense peak reported by [12] are E_x = 4.320, 4.443, 4.528, 5.050 MeV. These possibly correspond to E_x = 4.331, 4.454, 4.541, 5.060 MeV found in the present spectrum. Therefore, the present experiment agrees quite well with the past ^{91}Zr(p,d) experiment except for the ~10 keV calibration offset existing in their experiment.

3.3 Particle-γ coincidence for (p,t) spectrum

The same approach was taken for the ^{92}Zr(p,t) reaction. Fig. 4 a) shows a triton spectrum from the ^{92}Zr(p,t) reactions which is reconstructed by the same procedure as in the Fig. 3 a). Fig. 4 b) shows the simulated spectrum assuming the same energy resolution. As with the ^{91}Zr(p, d) case, the triton singles spectrum was reproduced well in energy although there exist some discrepancies in intensity.

Especially, the reduced intensity in the E_x = 2186 keV state is noticeable. This is possibly because the isomeric state of E_x = 2319 keV is not reconstructed in the present approach. The γ decay lifetime (τ = 809.2 ms) of the state is far longer than the particle-γ timing gate. In other words, the peak observed as the E_x = 2186 keV state is actually a doublet consisting of E_x = 2186 keV and 2319 keV states.

Figure 4. a) Estimated contributions from individual states to the ^{92}Zr(p,t) spectrum (see text for details). b) Simulated triton singles spectrum from the estimation (red) and actual triton singles spectrum (blue).

Figure 4 revealed the giant peak at E_x = 4.25 MeV consists of E_x = 4.331 (4+, 18%), 4.541 (6+, 18%), 4.124 (0+, 16%), 4.229 (2+, 10%), 4.681(2+, 10%), 4.814 and 4.818 (3 and 3,4+, 5% for two) MeV levels (percentages denote contributions to the peak). The peak at E_x = 5.0 MeV consists of E_x = 5.060 MeV (7+) and the peak at 5.5 MeV consists of E_x =5.457 (4+, 17%) and 5.513 MeV ((3,4), 15%). These peak structures can be compared with the ^{92}Zr(p,t) spectrum from [14]. Their spectrum was measured at 20° with 25 keV resolution using a 38 MeV proton beam. The intense peaks reported from the experiment are 4.125, 4.232, 4.335, 4.427, 4.543, 4.683, and 5.441 MeV. These definitely correspond to 4.124, 4.229, 4.331, 4.541, 4.681, and 5.457 MeV in the present spectrum. Despite the differences in measured angles and beam energy, the present spectrum agrees well with the past ^{92}Zr(p,t) experiment, and no significant mis-scaling in energy calibration is found from there.

3.4 Comparison of levels populated by ^{91}Zr(p,d) and ^{92}Zr(p,t) reactions

The states observed in either ^{91}Zr(p,d) or ^{92}Zr(p,t) reactions are summarized in Table 1 for comparison. Reaction dependence of populating these states is clearly observed and it can be seen that some states are populated by one reaction but not by the other. Although it is difficult to obtain a general trend about the reaction dependence from the present data, it seems that a high spin state such as $J = (7,8)\ \hbar$ is only populated by ^{91}Zr(p,d) and 0^+ states are only populated by ^{92}Zr(p,t) reaction. This may make sense considering the spin state of ^{91}Zr and ^{92}Zr ground states are $5/2^+$ (angular momentum: $L = 2\hbar$) and 0^+ ($L = 0\hbar$), respectively.

Table 1. The states of ^{90}Zr observed in either ^{91}Zr(p,d) or ^{92}Zr(p,t) reactions.
○ and × denote observed and unobserved (or possibly weakly populated), respectively.

E_x (keV)	J^π	^{91}Zr(p,d)	^{92}Zr(p,t)
1760	0^+	×	○
2319	5^-	×	○
4124	0^+	×	○
4229	2^+	×	○
4454	(5^+)	○	×
4640	$7,8$	○	×
4681	2^+	×	○
4992	2^-	○	×
5107	$3,4^+$	○	×
5426	3^-	○	×
5457	4^+	×	○
5513	$(3,4)^-$	×	○

4 Spin population in continuum region

4.1 γ-decay probability

In the highly-excited energy region (continuum region), we gain insights into the spins populated by the surrogate reactions by observing γ-decay probabilities, $P_i(E_x)$. $P_i(E_x)$ is a probability that the compound nucleus of interest (here ^{90}Zr), produced at a particular excitation energy E_x, decays via a specific γ-ray transition (i) that can be experimentally observed. This γ decay probability is given by

$$P_i (E_x) = (1 + a_{IC}) N_{P\text{-}\gamma}(E_x, i) / (\varepsilon(E_\gamma) N_{singles}(E_x)), \qquad (2)$$

where $N_{singles}$ gives the number of singles events (outgoing direct-reaction particle observed in detectors), $N_{P\text{-}\gamma}$ is the number of particle-γ coincidences observed for the transition of interest, ε denotes the γ-ray detection efficiency at the γ-ray energy E_γ, and a_{IC} gives the relevant internal conversion coefficient. $N_{singles}(E_x)$ is obtained from Fig. 1, while $N_{P\text{-}\gamma}(E_x)$ is the values obtained from the γ-ray spectrum gated on E_x by fitting a specific peak assuming a Gaussian shape. a_{IC} for the individual γ-rays were calculated using the software BRICC V. 2.0B [15].

4.2 Below the neutron separation energy

Fig. 5 shows $P_i(E_x)$ for the four discrete γ-ray transitions from ^{90}Zr low-lying states around E_x = 2-4 MeV as a function of excitation energies up to E_x = 20 MeV. The $P_i(E_x)$ typically show some peaks at low excitation energies which correspond to direct population of levels which decay via these γ-ray transitions. In the region of 7 MeV < E_x < S_n, the level density is so high that the highly-excited nuclear system that is produced in the surrogate (transfer or inelastic scattering) reaction mixes with the surrounding states and equilibrates, i.e. the intermediate nuclear system becomes a compound nucleus. We observe that the $P_i(E_x)$ are nearly constant in this high energy region. At excitation energies above S_n, the $P_i(E_x)$ drop to nearly zero because of the competition from neutron emission.

While the γ-ray transitions from low J states such as J = 2 $\hbar$ and 4 $\hbar$ show a similar trend indicating that the $P_i(E_x)$ are nearly independent of the reaction, the transitions from the higher J states such as J = 6 $\hbar$ and 8 $\hbar$ show significant reaction dependence and ^{90}Zr(p,p') shows notably smaller $P_i(E_x)$ than the other two reactions. These suggest that ^{90}Zr(p,p') does not populate as many high J ($\geqq$ 6 $\hbar$) states as ^{91}Zr(p,d) and ^{92}Zr(p,t) reactions. More complete results and discussion about the γ-decay probabilities can be found in [4].
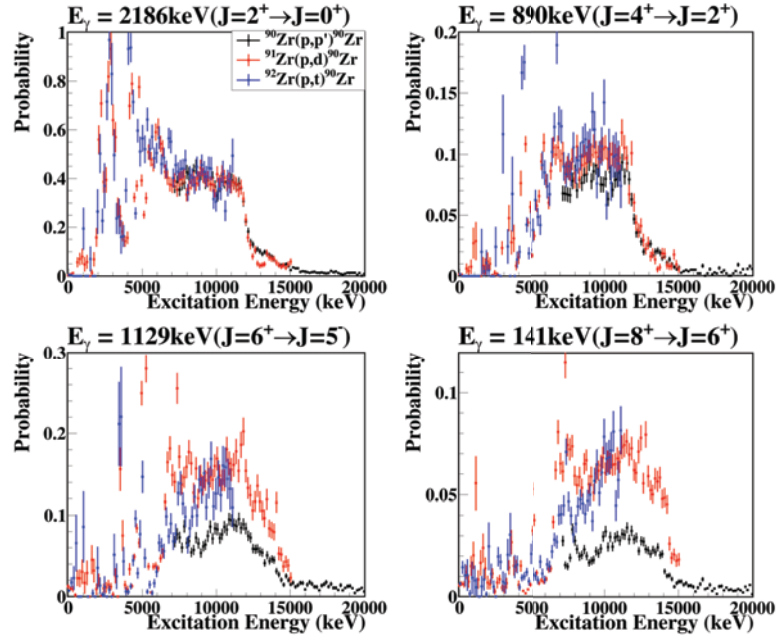
Figure 5. γ-decay probabilities for γ-ray transitions from different *J* states in ^{90}Zr (see [4] for more details).

4.3 Above the neutron separation energy

Figure 6 shows $P_i(E_x)$ for the γ-ray transitions from ^{89}Zr produced by neutron evaporation from ^{90}Zr compound nucleus produced by ^{90}Zr(*p,p'*), ^{91}Zr(*p,d*), and ^{92}Zr(*p,t*) (i.e., by ^{90}Zr(*p,p'n*), ^{91}Zr(*p,dn*), and ^{92}Zr(*p,tn*)) as a function of E_x in ^{90}Zr (the ^{92}Zr(*p,t*) data did not extend above S_n). $P_i(E_x)$ for γ-ray transitions in ^{89}Zr start to rise as the states become energetically accessible. The $P_i(E_x)$ above S_n show *J* dependence as was observed below S_n in section 4.2. While the ^{90}Zr(*p,p'n*) plot shows lower $P_i(E_x)$ than ^{91}Zr(*p,dn*) for high *J* states ($J^\pi = 9/2^+$ $\hbar$, $13/2^-$ $\hbar$), the ^{90}Zr(*p,p'n*) plot shows higher $P_i(E_x)$ than ^{91}Zr(*p,dn*) in γ-ray transtions from low *J* states such as $5/2^-$ $\hbar$ and $3/2^-$ $\hbar$. More complete results and a discussion of the γ-decay probabilities can be found in [4].
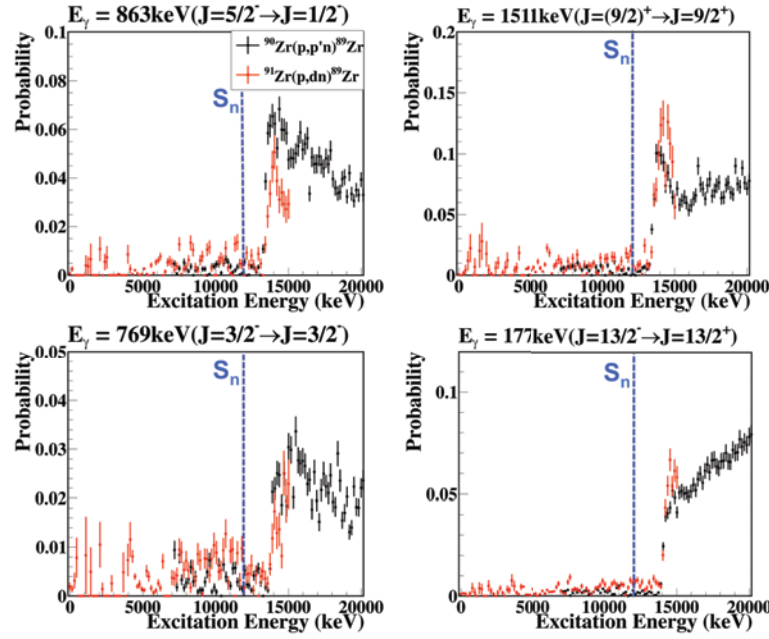
Figure 6. γ-decay probabilities for γ-ray transitions from different J states in ^{89}Zr (see [4] for more details).

5 Summary and Outlook

The ^{90}Zr nucleus spin distribution produced by three different reactions, namely (p,p'), (p,d), and (p,t) reactions were studied. The outgoing particles were detected in coincidence with γ-rays emitted by the ^{89,90}Zr nuclei. These data, especially the spin populations around the neutron separation energy (S_n), can be used to understand the decay of the compound nucleus formed in ^{89}Zr(n,γ). The γ decay probabilities, $P_i(E_x)$, are crucial to develop theoretical models for determining (n,γ) cross sections using the present surrogate reaction approach.

The low-lying states of ^{90}Zr at $E_x < 6$ MeV observed in the present (p,d), and (p,t) experiments agreed well with the past measurements. Although it is difficult to obtain a general trend for the reaction dependence from the present data in the energy region, it seems s that a high spin state such as $J = (7,8)\,\hbar$ is only populated by ^{91}Zr(p,d) and 0^+ states are only populated by ^{92}Zr(p,t) reaction. This may make sense considering the spins of the ^{91}Zr and ^{92}Zr ground states are $5/2^+$ (angular momentum: $L = 2\hbar$) and 0^+ ($L = 0\hbar$), respectively.

We carried out measurements of $P_i(E_x)$ for γ-rays emitted in the decay of ^{90}Zr nucleus produced near S_n. We observed that the ^{90}Zr(p,p') reaction produces notably fewer γ-rays from high J states than the ^{91}Zr(p,d) and ^{92}Zr(p,t) reactions. This suggests the inelastic scattering preferably populates lower J states in ^{90}Zr than the transfer reactions. This reaction dependence holds over several MeV above S_n.

Quantitative study regarding the J^π population of the ^{90}Zr compound nucleus and ^{89}Zr(n,γ) cross sections from the surrogate reaction approach will be forthcoming.

Acknowledgement

References

1. J. E. Escher, J. T. Burke, F. S. Dietrich, N. D. Scielzo, I. J. Thompson, and W. Younes, Rev. Mod. Phys. 84, 353 (2012)
2. N. D. Scielzo, J. E. Escher, J. M. Allmond, M. S. Basunia, C. W. Beausang, L. A. Bernstein, D. L. Bluel, J. T. Burke, R. M. Clark, F. S. Dietrich, P. Fallon, J. Gibelin, B. L. Goldblum, S. R. Lesher, M. A. McMahan, E. B. Norman, L. Phair, E. Rodriquez-Vieitez, S. A. Sheets, I. J. Thompson, and M. Wiedeking, Phys. Rev. C 81, 034608 (2010).
3. S. Ota, J. T. Burke, R. J. Casperson, J. E. Escher, R. O. Hughes, J. J. Ressler, N. D. Scielzo, I. J. Thompson, R. A. E. Austin, E. McCleskey, M. McCleskey, A. Saastamoinen, and T. Ross, EPJ Web Conf. 93, 02001 (2015).
4. S. Ota, J. T. Burke, R. J. Casperson, J. E. Escher, R. O. Hughes, J. J. Ressler, N. D. Scielzo, I. J. Thompson, R. A. E. Austin, B. Abromeit, N. J. Foley, E. McCleskey, M. McCleskey, H. I. Park, A. Saastamoinen, and T. J. Ross, Phys. Rev. C 92, 054603 (2015).
5. R. Schwengner, G. Rusev, N. Tsoneva, N. Benouaret, R. Beyer, M. Erhard, E. Grosse, A. R. Junghans, J. Klug, K. Kosev, H. Lenske, C. Nair, K. D. Schilling, and A. Wagner, Phys. Rev. C 78, 064314 (2008).
6. A. C. Larsen, M. Guttormsen, M. Krticka, E. Betak, A. Burger, A. Gorgen, H. T. Nyhus, J. Rekstad, A. Schiller, S. Siem, H. K. Toft, G. M. Tveten, A. V. Voinov and K. Wikan, Phys. Rev. C 83, 034315 (2011).
7. D. Savran, T. Aumann, A. Zilges, Prog. Part. Nucl. Phys. 70, 210-245 (2013).
8. L. Netterdon, A. Endres, S. Goriely, J. Mayer, P. Scholz, M. Spieker, A. Zilges, Phys. Lett. B 744, 358-362 (2015).
9. J. E. Escher and F. S. Dietrich, Phys. Rev. C 81, 024612 (2010).
10. J. E. Escher et al., EPJ Web Conf. (in this issue).
11. S. R. Lesher, L. Phair, L. A. Bernstein, D. L. Bleuel, J. T. Burke, J. A. Church, P. Fallon, J. Gibelin, N. D. Scielzo, and M. Wiedeking, Nucl. Instrum. Methods Phys Res., Sect. A 621, 286 (2010).
12. J. B. Ball and C. B. Fulmer, Phys. Rev. 172, 1199 (1968).
13. P. E. Garrett, W. Younes, J. A. Becker, L. A. Bernstein, E. M. Baum, D. P. DiPrete, R. A. Gatenby, E. L. Johnson, C. A. McGrath, S. W. Yates, M. Devlin, N. Fotiades, R. O. Nelson, and B. A. Brown, Phys. Rev. C 68, 024312 (2003).
14. J. B. Ball, R. L. Auble, and P. G. Roos, Phys. Rev. C 4, 196 (1971).
15. T. Kibedi, T. W. Burrows, M. B. Trzhaskovskaya, P. M. Davidson, and C. W. Nestor, Nucl. Instrum. Methods Phys. Res., Sect. A 589, 202 (2008).